JOURNAL OF AIRCRAFT
Vol. 37, No. 5, September–October 2000

Aeroservoelastic Analysis of the B-2 Bomber

Robert T. Britt,* Steven B. Jacobson,† and Thomas D. Arthurs‡
Northrop Grumman Corporation, Pico Rivera, California 90660

In the early stages of the development of the B-2 bomber, the technical challenges posed by the aeroelastic characteristics of the all-wing aircraft were recognized. The configuration's near-neutral pitch stability and light wing loading made the aircraft highly responsive to atmospheric turbulence. This dictated the requirement for an active digital flight control system to provide both stability augmentation and gust load alleviation. The gust load alleviation flight control system was designed by a multidisciplinary team using a combination of optimal and classical control design techniques. The analytical models included linearized approximations of the digital control law mechanization. Flight-test data analysis included the extraction of the vehicle open-loop response, which compared well with the analytical predictions. The multidisciplinary design approach resulted in the successful development of a control augmentation system that provides the B-2 with superb handling characteristics, acceptable low-altitude ride quality, and substantial alleviation of gust loads on the airframe.

Nomenclature

$A(k)$	=	generalized aerodynamic matrix
BM_i	=	bending moment response at ith station
$\bar{c}$	=	Mean aerodynamic chord, ft
j	=	square root of (-1)
k	=	reduced frequency, $\bar{c} \times \omega / 2 \times V$
q	=	pitch rate
s	=	Laplace variable, $j \times \omega$
V	=	velocity, ft/s
z	=	plunge generalized coordinate
δ_i	=	control surface positions
η_i	=	ith elastic generalized coordinate
θ	=	pitch generalized coordinate
ω	=	circular frequency, rad/s

Introduction

EARLY in the full-scale development of the B-2 bomber, it was recognized that active flight control technology would be required to provide gust load alleviation because of the aircraft's relatively light wing loading and the requirement to fly low-altitude, high-speed, terrain following missions. Preliminary analyses indicated that gust loads would constitute the primary design load conditions for much of the inboard wing and carry-through box structure. Design goals for the flight control gust load alleviation (GLA) system included good ride quality, platform stability for weapons deployment, and a significant reduction of structural loads in turbulence. The design effort required a multidisciplinary team approach involving structural dynamics, aeroelasticity, and flight control specialists.

Overall air vehicle design activities included refinement of the planform configuration and the design and placement of control surfaces with the required control authority to meet flying qualities and GLA objectives. Flight control system design activities included selection and placement of appropriate sensors, definition of actuator force, rate and bandwidth requirements, and synthesis of the control laws. Dynamic response and flutter analysis activities included development of the aeroelastic models that would be the basis for the GLA design and verification of GLA performance with respect to structural loads and aeroservoelastic stability. A common analytical model database was utilized by all disciplines to ensure consistent, adequate performance for the final design. This paper discusses elements of model development, methodologies used to design the GLA control system, and analyses used to define gust design load requirements and verify aeroservoelastic stability. Flight-test results that validated the final system design are also discussed.

Received 24 August 1998; revision received 1 August 1999; accepted for publication 6 September 1999.

*Manager, B-2 Flight Sciences, Military Aircraft Systems Division, 8900 East Washington Boulevard. Senior Member AIAA.

†Senior Technical Specialist, B-2 Flight Controls, Military Aircraft Systems Division, 8900 East Washington Boulevard.

‡Vice President, Engineering Technology and Development, Military Aircraft Systems Division, 8900 East Washington Boulevard. Fellow AIAA.

B-2 Overview

The B-2 is an all-wing, high-subsonic aircraft that utilizes three sets of elevons for combined pitch and roll control, a centerline gust load alleviation surface (GLAS) for pitch control, and upper and lower split drag rudders for yaw control. The structural configuration includes a dual carry-through box construction with large cutouts and cavities housing the propulsion system and weapons bay. A substantial amount of the airframe is fabricated from fiber composite materials. The planform and airfoil design are dictated from a combination of aerodynamic performance, control authority, and low observables requirements. The aircraft employs a full-time active flight control stability augmentation system.

Figure 1 shows a schematic of the quad redundant flight control architecture and major components. The B-2 can be flown with any one of the four channels operational. The feedback sensors used for active stability augmentation include the air data system to measure the flight condition, aerodynamic angle of attack, and sideslip and the attitude motion sensor set (AMSS) to provide inertial response data.

The flight control computers (FCCs) are the brains of the flight control system. The FCCs' functions include 1) computing surface position commands in response to the feedback sensor inputs, pilot commands, and guidance commands; 2) input signal management fault detection, fault isolation, and selection; and 3) interface with the avionics systems.

The flight control actuation system[1] includes 24 actuators and 2 sets of quadraplex actuator remote terminals (ARTs). At least 2 actuators drive each of the 11 primary control surfaces. Each actuator is powered by two different hydraulic systems so that each control surface is connected to all four hydraulic systems. The centerline GLAS is the only exception and is plumbed to only two hydraulic systems.

Analytical Models

Structural Modeling

Basic structural and aerodynamic modeling was carried out in the MSC/NASTRAN[2] finite element modeling system. The majority of dynamic analyses utilized half-span models. Separate symmetric

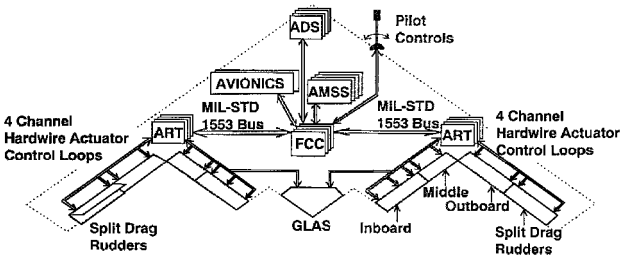

Fig. 1 Flight control architecture.

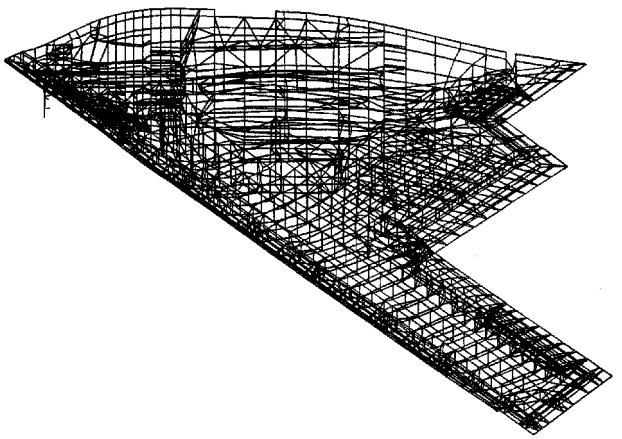

Fig. 2 Half-span finite element model.

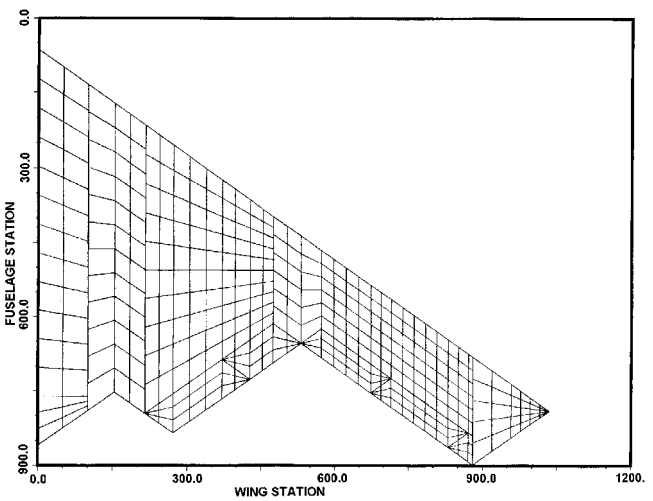

Fig. 3 Doublet lattice model.

and antisymmetric response analyses were accomplished by inserting the appropriate centerline boundary conditions. A high-order stress model was reduced for dynamic analyses and included over 10,000 elements, 3800 grid points, and a reduced analysis set of 631 degrees of freedom (Fig. 2). A simpler beam finite element method (FEM) was constructed for use in the many parametric analyses. Extensive checking was performed to verify that the reduced-order dynamic models adequately represented the basic dynamic characteristics of the airframe as predicted by the high-order FEM. These included force and deflection characteristics, frequencies, mode shapes (and node lines), strain energy distributions, and generalized mass.

Aerodynamic Modeling

The subsonic aerodynamic forces for both motion and gust-induced angle of attack were generated from a half-span 384 box model (Fig. 3) developed to satisfy reduced frequency requirements for both flutter and dynamic gust response analyses. The two-dimensional doublet lattice method (DLM) was selected to develop the unsteady forces. Correction factors[3] were generated to ensure that the spanwise distributions predicted by the DLM model matched those derived from wind-tunnel test data for steady flow conditions. Similar corrections were made to control surface induced pitching moment increments by applying factors to surface commands as part of the control system modeling.

Frequency Domain: State-Space Conversion

MSC/NASTRAN was utilized to generate the basic data necessary to transform the second-order frequency domain equations of motion into a state-space system. Generalized mass, stiffness, and aerodynamic matrices (both motion dependent and gust disturbance) were the starting point for this model. A subset of the physical degrees of freedom in the mode shapes was provided at locations of interest so that physical motions could be recovered to define sensor feedback outputs and forces developed by the actuation system. Bending moment modal coefficient data were also provided.

Conversion into a state-space formulation[4] requires a frequency domain approximation of the doublet lattice aerodynamics. The generalized aerodynamic matrix $A(k)$ at m values of reduced frequency can be approximated[5] by the summation of a finite number of functions $f_j(\omega)$ where $j = 1\text{-}p$. The general form is

$$A(\omega) = A_1 f_1(\omega) + A_2 f_2(\omega) + \cdots + A_p f_p(\omega) \tag{1}$$

Generally, the applicable functions for use in the approximation are given by

$$f_1(\omega) = s^2 = -\omega^2, \qquad f_2(\omega) = s = j\omega, \qquad f_3(\omega) = 1$$

$$f_4(\omega) = s/(s + \lambda_1) = j\omega/(j\omega + \lambda_1)$$

$$f_5(\omega) = s/(s + \lambda_2) = j\omega/(j\omega + \lambda_2) \tag{2}$$

Exceptions to the general case are as follows:

1) The first two columns (plunge and pitch) of the aerodynamic matrix, which are fit without the $f_1(\omega)$ term.

2) The last column (gust), which is fit without the first two terms [$f_1(\omega)$ and $f_2(\omega)$], but with the addition of two more high pass terms, $f_6(\omega) = s/(s + \lambda_3)$ and $f_7(\omega) = s/(s + \lambda_4)$.

3) The $f_3(\omega)$ (constant) term of the last column, which is forced to have the same coefficient (a_3) as the first column.

After determining $A(\omega)$, using a least-squares fit solution, the second-order system is transformed into the familiar state-space formulation:

$$\dot{x} = A \times x + B \times u \tag{3}$$

$$y = C \times x + D \times u \tag{4}$$

where, for the B-2 analysis,

$$x = [z, \theta, \eta_1, \eta_2, \ldots, \eta_{nf}, \delta_1, \delta_2, \ldots, \delta_{nu},$$

$$\dot{z}, \dot{\theta}, \dot{\eta}_1, \dot{\eta}_2, \ldots, \dot{\eta}_{nf}, \dot{\delta}_1, \dot{\delta}_2, \ldots, \dot{\delta}_{nu}]^T$$

$$u = [\delta_1 \delta_2 \delta_3 \delta_4 w_{\text{gust}}]^T$$

$$y = [N_Z, q, \alpha, BM_0, BM_1, \ldots, BM_n.\delta_1, \delta_2.\delta_{nu}, \dot{\delta}_1 \dot{\delta}_2, \ldots, \dot{\delta}_{nu}]^T$$

The resulting analog state-space models retain 2 rigid-body (pitch and plunge) modes, 16 flexible modes, 4 control surface inputs, and a gust disturbance input. The analog state-space models generally have about 100 states. Excellent agreement between the MSC/NASTRAN frequency domain solution and the state-space model was achieved, as seen from the comparisons of Figs. 4 and 5.

Actuator Modeling

A model of the actuation system was included in both the MSC/NASTRAN formulation and the state-space model. The actuator was modeled to apply a force between the control surface and the backup structure. The structural model included coincident grid

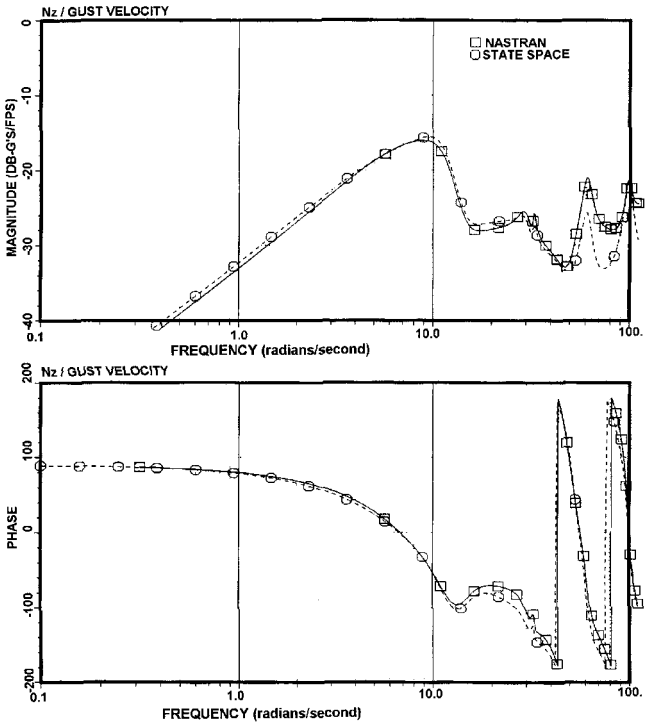

Fig. 4 *Nz* **response due to gust.**

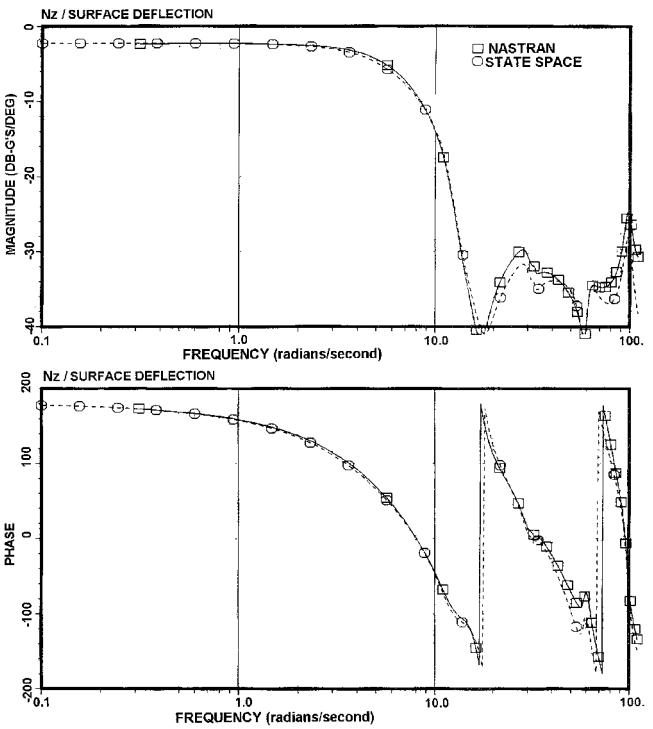

Fig. 5 *Nz* **response to inboard elevon.**

points to allow relative motion between the control surface and primary structure. In MSC/NASTRAN the multipoint constraint feature is used to define relative motion using scalar point degrees of freedom. The block diagram in Fig. 6 shows the general form of the model.[1] The actuator includes an outer position control loop and a dynamic pressure feedback control loop to dampen the control surface resonance modes. Extra point degrees of freedoms are used to define other block diagram variables. The transfer function (TF) option is used to define the actuator model in MSC/NASTRAN. Figure 7 shows the actuator and surface response to command, illustrating the surface dynamics included in the model.

GLA Summary

GLA control of the B-2 involves quickly pitching the aircraft into the gust to control the buildup of gust angle of attack and thereby minimize normal acceleration and structural loads. Effective GLA performance requires a high bandwidth pitch control augmentation system with high control surface rates.

Figure 8 shows an example of the centerline bending moment GLA performance achieved on the B-2. Generally, the GLA controller performance reduces incremental gust loads by up to 50% when compared to an open-loop (unaugmented) model or a closed-loop handling qualities controller design. Similar ride quality improvements are also attained.

Analysis of the lateral/directional axes showed more conventional, nearly rigid responses with adequate separation of the required controller bandwidths and antisymmetric flexible mode frequencies. Lateral GLA was not required due to the low projected side area. The lateral directional flight control laws were, therefore, developed with simpler quasi-elastic models and successfully verified during a flight test.

Digital Effects

Early flight control analysis showed that the high bandwidth required for effective GLA performance was sensitive to the phase degradation of feedback signal data latency and digital implementation. To minimize these effects, a bottom up approach was taken to define performance and throughput requirements for the sensors, MIL-STD-1553 multiplex bus traffic and timing, FCC timing and throughput calculations, actuator bandwidths, and surface rates.

Feedback signal data latency was defined and included in the digitized models as partial and full frame delays. Feedback data latency is the finite time delay, measured from the analog air vehicle motion or state feedback through the FCC surface command calculations to the actuator command at the ARTs. The digital response in Fig. 9 shows the phase lag due to throughput and digitization effects compared to the analog response.

Analog filters were developed to approximate the ratio of the open-loop digital and analog model frequency responses. These filters were then applied to the MSC/NASTRAN analog model to approximate the GLA performance with the digital and throughput delay effects. Figure 9 shows how well these analog filters adequately approximate the digital model response up to 70 rad/s, which is well beyond the GLA controller frequency range of interest. Flutter analyses included additional filters to assess the impact of phase shifts beyond this frequency.

GLA Controller Development

The pitch control augmentation system (PCAS) GLA synthesis utilized classical and modern control theory methods. Piloted simulation was used to verify and adjust, as required, the predicted handling qualities.

Power spectral density (PSD) and rms response to the MIL-STD-8785C Dryden turbulence model were the primary analysis techniques used to evaluate the GLA performance. Hybrid statistical analysis techniques[6] were also employed to evaluate the analog vehicle response with a digital controller. Ride qualities criteria for the B-2 bomber are outlined in Ref. 7.

Optimal controller results were used to bound the achievable GLA performance and focus development of a classical multiple-input/multiple-output (MIMO) design. Each feedback loop was confirmed by classical analyses and a solid physical understanding before implementation. This quickly eliminated many ineffective optimal gains and retained the available elevon surface rates for the best control loop GLA performers.

The B-2 PCAS achieves consistent level 1 handling qualities throughout the flight envelope using a load factor and pitch rate proportional plus integral (NZQPPI) design. GLA performance is achieved with a combination of NZQPPI low-frequency control and a gust sniffer loop for mid- and high-frequency control. The gust sniffer loop senses the aerodynamic gust angle of attack by subtracting the inertial angle of attack from the total (inertial plus gust)

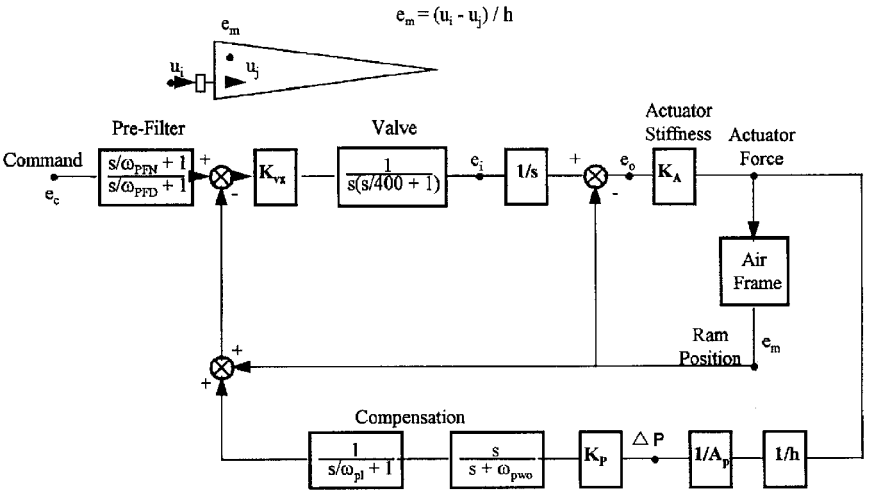

Fig. 6 Actuator model.

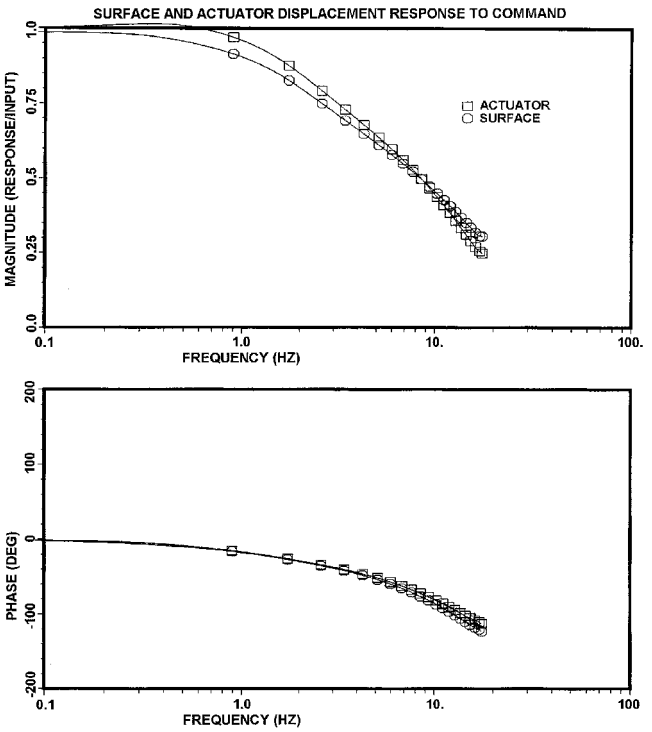

Fig. 7 Surface response to command.

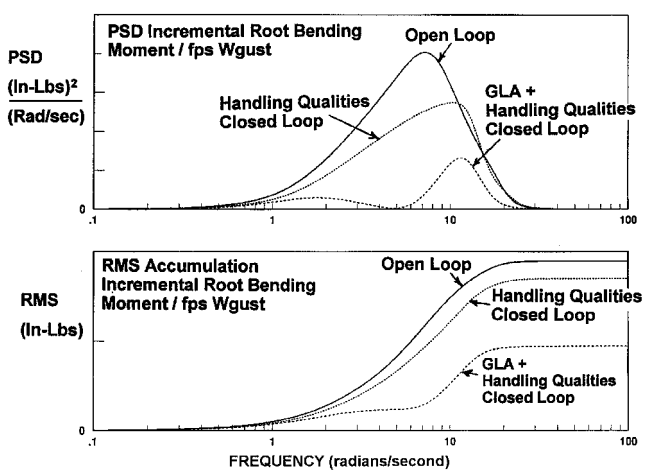

Fig. 8 GLA performance.

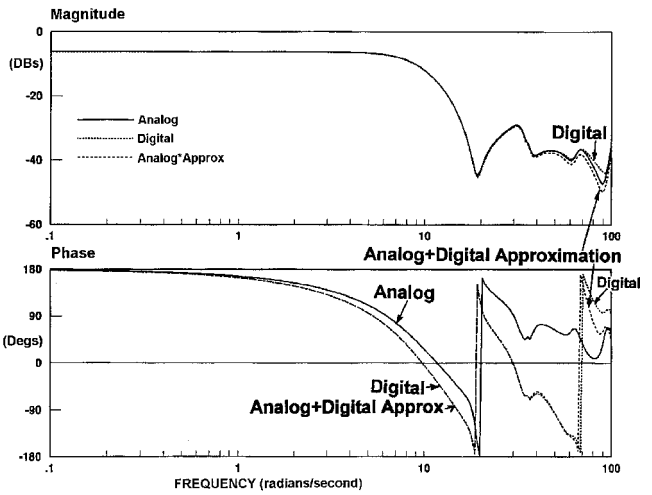

Fig. 9 Open-loop pitch rate to inboard elevon.

aerodynamic angle of attack at the nose. Feedback gains, loop shaping compensation, and surface utilization mixing are scheduled with flight condition.

Pitch Control Surface Utilization

Innovative pitch control surface mixing is used to provide active flexible mode damping at low and high altitudes. Figure 10 shows the node line of the first flexible symmetric mode. Aggressively pitching the B-2 into vertical gusts at low altitude using the GLAS and inboard elevons significantly reduces the low-frequency, rigid-body gust response, but tends to excite the first flexible mode. Because the outboard elevon is outboard of the node line, commanding it out of phase with respect to the inboard elevon dampens the first flexible mode response. The outboard elevon also provides local high-frequency direct lift control by decambering the local wing chord.

Reduced aerodynamic damping at high altitude produced a significant flexible mode contribution to the total pitch control loop for heavy outboard fuel conditions. An innovative control surface mixing concept, referred to as the inertial damper, was developed to minimize the excitation of and dampen the first flexible mode, while still maintaining the required control loop bandwidth. Although classical notch filter loop shaping could have attenuated the flexible mode, the additional phase lag incurred would have adversely affected the closed-loop short period handling qualities. At high altitudes, the centerline GLAS appears more effective inertially than aerodynamically. The inertial damper surface mixing uses the

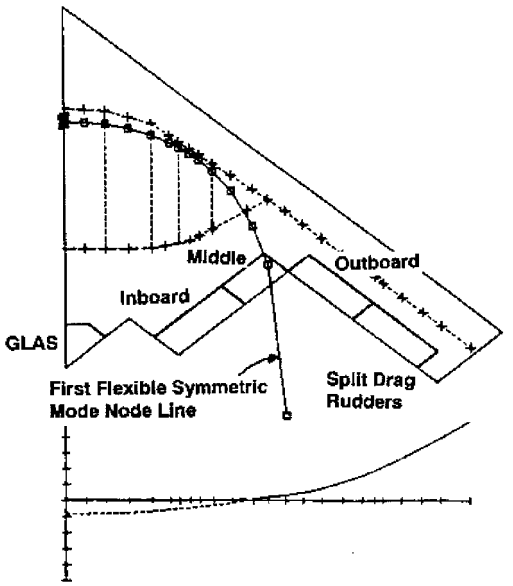

Fig. 10 First flexible symmetric mode.

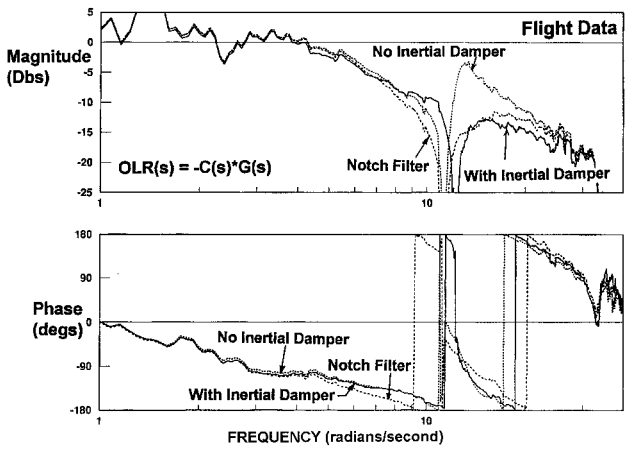

Fig. 11 High-altitude inertial damper.

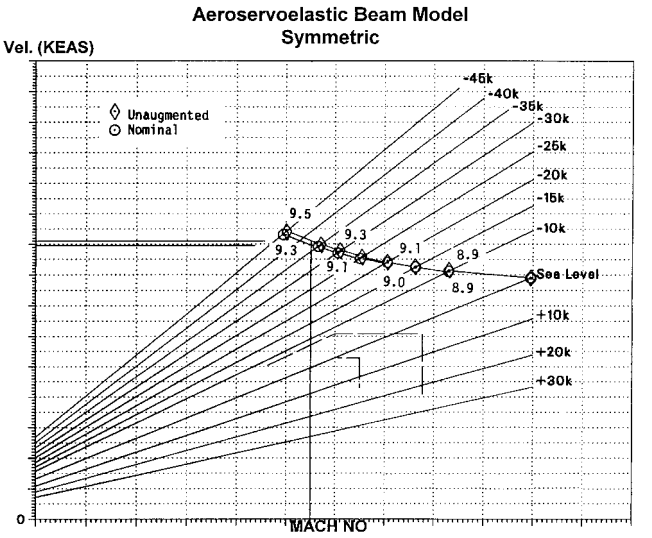

Fig. 12 Matched point flutter results.

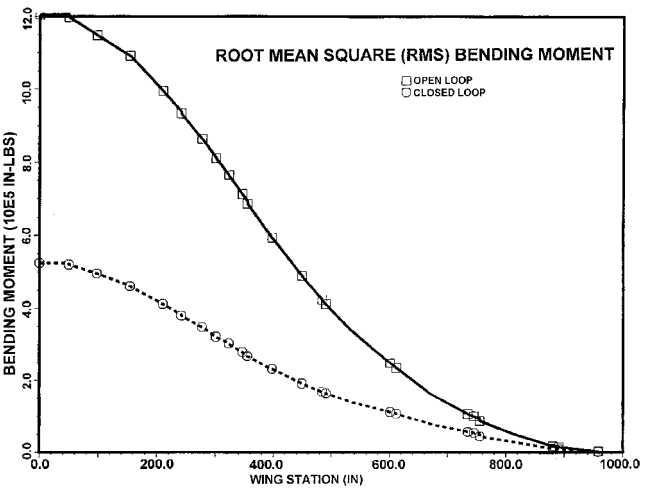

Fig. 13 Spanwise bending moment.

GLAS out of phase with a bandpass filter to attenuate the inboard elevon flexible mode excitation and a small amount of high-pass filtered outboard elevon in phase to recoup the aerodynamic control power. Flight test data in Fig. 11 show how the inertial damper surface mixing achieves the desired flexible mode gain attenuation without incurring the additional phase lag from a classical notch filter implementation.

Flutter Analysis

Matched point flutter analyses were performed using the PK solution in MSC/NASTRAN. Both symmetric and antisymmetric analyses were conducted. Complete parametric analyses varying fuel, payload, and other parameters were conducted to understand basic flutter characteristics. The spanwise stiffness distribution of the graphite composite wing box of the B-2 was tailored to achieve a wide separation between the fundamental bending and torsion frequencies. As a consequence, the basic flutter speeds were predicted to be well outside of the required flutter boundary.

Matched point flutter analyses including the active flight control system were also performed using the PK solution procedure. The closed-loop system was included in the analysis, using extra points and TF modeling features.

Figure 12 presents a match point symmetric flutter analysis comparing results between the open-loop and nominal flight control system. A significant change in results for bending/torsion flutter was not expected because the bandwidth of the controller did not extend beyond the frequency of the first symmetric structural mode. Careful consideration was given to the coupling between rigid-body pitch and the first flexible mode.

Gust Design Loads Analysis

Design load requirements were derived from continuous turbulence analysis criteria.[8] Gust loads developed from PSD analyses are greater than maneuver requirements over a significant portion of the inboard wing. Development of gust design loads was carried out in MSC/NASTRAN and included the active GLA system.

Airframe loads (shear, bending moment, and torque) were calculated using load integration matrices that operate on grid point forces generated from the stiffness matrix and the computed deflections. This calculation is performed in MSC/NASTRAN, using a user input program DMAP in the frequency domain, thus assuring the correct phasing of the forces in the integration. Figure 13 shows a bending moment comparison between GLA on and off for a nominal flight condition. A significant reduction in loading has been achieved across the entire span of the wing.

Considerations related to the development of phased load design conditions for structural analysis followed approaches similar to those in Ref. 9. Effects of control system nonlinearities at peak gust conditions were included, also in a manner similar to those in Ref. 9. Nonuniform spanwise gust effects have also been examined for the B-2 (Ref. 10).

Ground Vibration Test

A full-scale ground vibration test was one element of the flutter clearance program. Four weight configurations were tested. The vehicle was suspended on a soft support system and sufficient instrumentation included to measure the vehicle mode shapes in the frequency range of interest. A ground resonance test was also conducted at this time.

Posttest analysis included a structural model revision to achieve closer test/analysis frequency correlation. Complex structural configurations like the B-2, simulated by a complex FEM, do not lend themselves to simple changes but usually require utilizing results of sensitivity analyses to change frequencies and mode shape.

A check of the analytical mass distribution was made by checking the orthogonality between the test modes. The first several modes exhibited good orthogonality, and no changes were made in the mass distribution.

A stiffness modification approach was implemented utilizing an optimization program to determine stiffness changes. Design parameters were first defined consisting of groups of element stiffnesses, areas, or thicknesses. MSC/NASTRAN's design sensitivity solution (solution 53) was executed to compute parameter sensitivity coefficients for each modal frequency. The CONMIN[11] optimization program was run to minimize a cost function:

$$\text{Cost} = \left[\sum_{i=1}^{n} (\omega_{Ai} - \omega_{Ti})^2 \right] \tag{5}$$

where n is the number of modes, ω_A the analysis frequency, and ω_T the test frequency.

The optimization provided several candidate solutions depending on constraints imposed on design parameter allowable changes. The final solution was selected based on the best match with both frequency and mode shape data. The revised model was then used in all subsequent dynamic analyses.

Flight Testing

Flight testing was conducted to verify that flutter, flying qualities, and other dynamic response characteristics were satisfactory. Because of the highly augmented flight control design, integrated flight control and flutter flight testing was required during envelope expansion. Test maneuvers at 1 g were performed first to verify stability and handling. Flutter excitations followed with near-real-time analysis. Elevated-g flight control maneuvers then followed after clearance from the flutter analysis.

The vehicle was dynamically excited by oscillating the control surfaces. This was accomplished with pilot pitch and roll stick inputs or by special test hardware [flight control test panel (FCTP)] mounted in the cockpit. The bandwidth of the actuation system, together with the size of the B-2 control surfaces, was sufficient to provide effective excitation of the air vehicle. Figure 14 shows the coherence function between the surface displacement and an outboard wing strain gauge response.

Data were simultaneously recorded on the aircraft and telemetered to the ground station for display, real-time processing, and postflight analysis. A flutter data analysis test system[12] was developed to perform near-real-time and postflight analysis.

The system featured three methods for estimating frequency and damping; however, one method, the Sanathanan parameter estimation technique[13] (SPET), was the primary analysis tool. This method demonstrated several advantages over the other methods. The SPET fits polynomial coefficients of a frequency response function $G(j\omega)$ represented as the ratio of two complex polynomials [Eq. (6)]. The number of poles and zeros is user selectable. A curve fit is performed to obtain the fitted numerator and denominator polynomial coefficients, and then an optimization technique is employed to minimize the error between the acquired TF and the theoretical frequency response. The roots of the denominator are then determined to obtain frequencies and damping. The SPET was capable of fitting multiple modes over a wide frequency range and could simultaneously fit closely spaced modes. Both were important under the time constraints of performing near-real-time analysis to support point-to-point clearance during flight tests:

$$\text{FRF} = G(j\omega) = P(j\omega)/Q(j\omega) \tag{6}$$

Figure 15 compares a frequency response function (FRF) for a midspan normal accelerometer with curve fit results using the SPET. Near-real-time analysis focused on a subset of the available instrumentation, whereas postflight analysis considered the entire instrumentation suite.

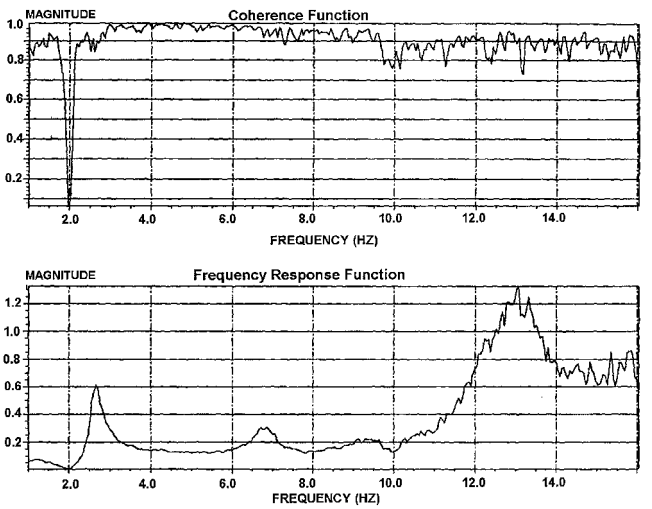

Fig. 14 Coherence function and strain gauge FRF.

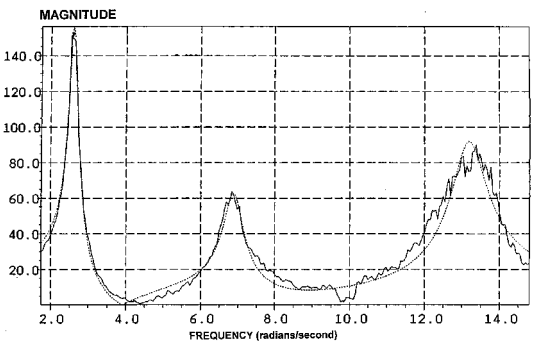

Fig. 15 Accelerated FRF with curve fit.

Flight-Test Matching/Model Update

Typically, it is both difficult and tedious to extract accurate, open-loop, MIMO model data from heavily augmented closed-loop test results. Full-time active flight control augmentation requirements prohibited testing with the augmentation disengaged. Control surface effectiveness, surface mixing, and short period/flexible mode interaction are important to both the B-2's high altitude inertial damper and low-altitude, high-speed GLA performance. Verification of the accuracy of the open-loop aeroservoelastic model, therefore, was necessary.

Typical parameter identification analysis methods have either emphasized specific state-space model formats with a fixed number of rigid-body and flexible modes or extraction of specific aerodynamic coefficients. B-2 flight test data parameter identification and model matching attempts using NASA's modified maximum likelihood estimator[14] (MMLE3) program gave inconsistent results, with wide variations in model estimates between very close flight conditions, for all except the basic coefficients.

B-2 parameter identification was further complicated by the sensitivity of the closely coupled short period and wing first symmetric bending modes to differential motions between the structural (sensor) and mean inertial axes.[15] Although early flight-test results verified basic aeroelastic stability and flying quality performance,

detailed correlation with the analytical models indicated that some aerodynamic terms required adjustments.

The flight data verification effort for the B-2 bypassed the difficulties and limitations experienced in the past by directly developing open-loop frequency-domain flight data models (FDMs), $G(s)$ from the closed-loop responses. The open-loop FDMs permitted direct frequency-domain comparisons with the aeroservoelastic models, closed-loop design performance verification, and flight-test-based analysis confirming proposed design adjustments. Quasi-steady, low-frequency (wind upturn) flight-test results compared reasonably well with predicted wind-tunnel data. The FDMs successfully captured the effects of the unsteady aerodynamics and flexible vehicle interaction for the midfrequency range near and around the short period and first symmetric flexible mode. The high-altitude inertial damper was efficiently tuned using the open-loop FDMs.

Figure 16 shows the open- and closed-loop MIMO FDM frequency response matrix format. Closed-loop time response flight-test data to individual pitch control surface random excitations were collected using the FCTP. High-coherency frequency responses of the closed-loop outputs to the known random surface excitations were then constructed during postflight analysis and included in the appropriate column of the closed-loop frequency response matrix $Gcl(s)$. $C(s)$ is the constant MIMO controller for the tested condition. By keeping the vehicle configuration and flight condition constant, the only unknown in the closed-loop equation is the open-loop frequency response $G(s)$, shown in Fig. 16.

The vehicle configuration gross weight, center of gravity, and fuel distribution were kept approximately constant by collecting all of the necessary individual surface excitations for a given flight condition in rapid succession. The flight condition was kept constant by using the autopilot to maintain pitch attitude and, thereby, trim altitude and angle of attack. The pilot's only task was to maintain the desired speed condition using slow smooth throttle movements. Keeping the pilot's hands off the stick eliminated any disturbances in the closed-loop response due to unknown and adaptive human pilot control loop inputs.

The open-loop MIMO FDM compared well with the open-loop quasi-elastic (rigid plus elastic corrections) and aeroservoelastic models. Increased pitch stability and variations in individual surface effectiveness were noted. Comparisons were also made of the total pitch control open-loop return (OLR) [$\mathrm{OLR} = -C(s) \times G(s)$] developed from a single-pilot pitch frequency sweep and the open-loop FDM. Figure 17 shows a good match between approximately 2 and 40 rad/s, which was the frequency range of interest and where the individual surface excitation power was concentrated. The open-loop FDM degrades below 2 and above 40 rad/s (as expected) due to insufficient excitation power and subsequent poor signal-to-noise ratios. Good checks were generally available with surface excitations that produced approximately $\pm 0.6\ g$ at the AMSS while in very little to no turbulence and approximately constant flight conditions and

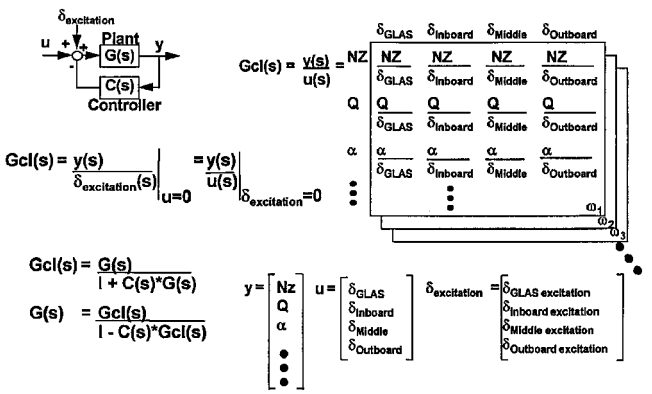

Fig. 16 Flight data model extraction.

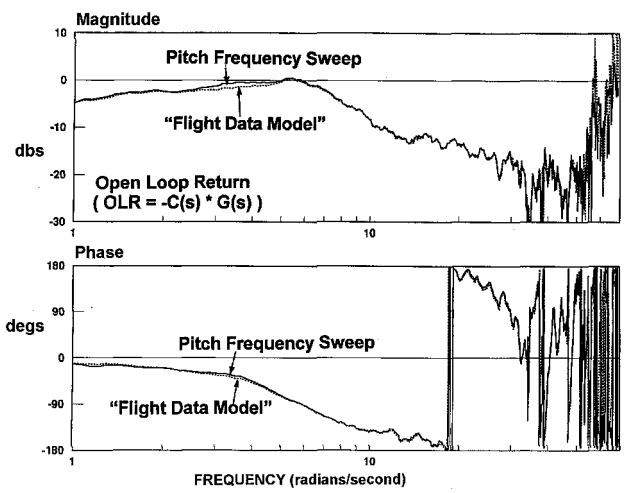

Fig. 17 Good comparison FDM.

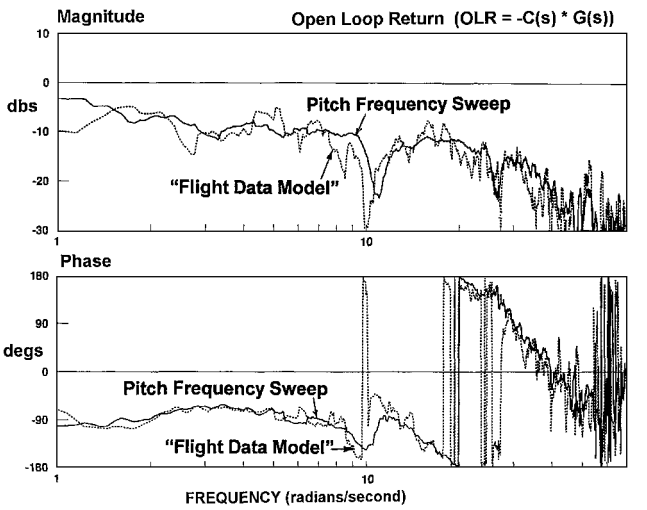

Fig. 18 Poor comparison due to turbulence.

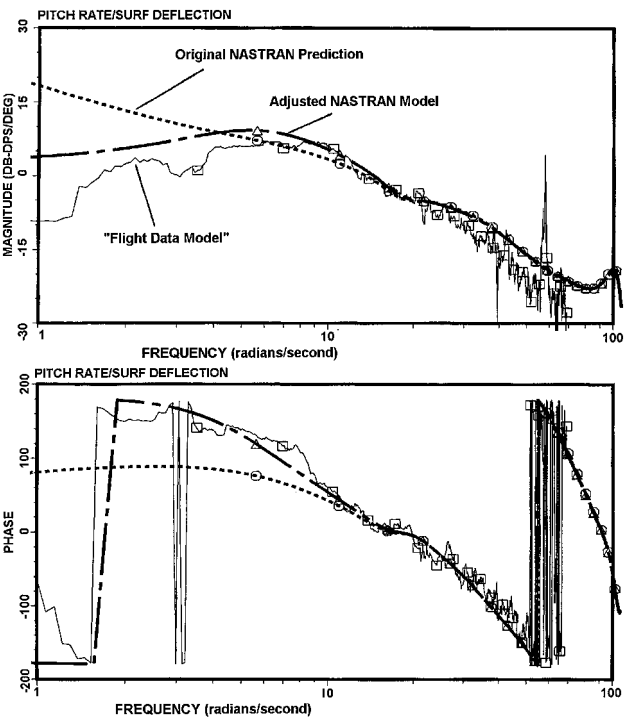

Fig. 19 Open-loop pitch rate to inboard elevon.

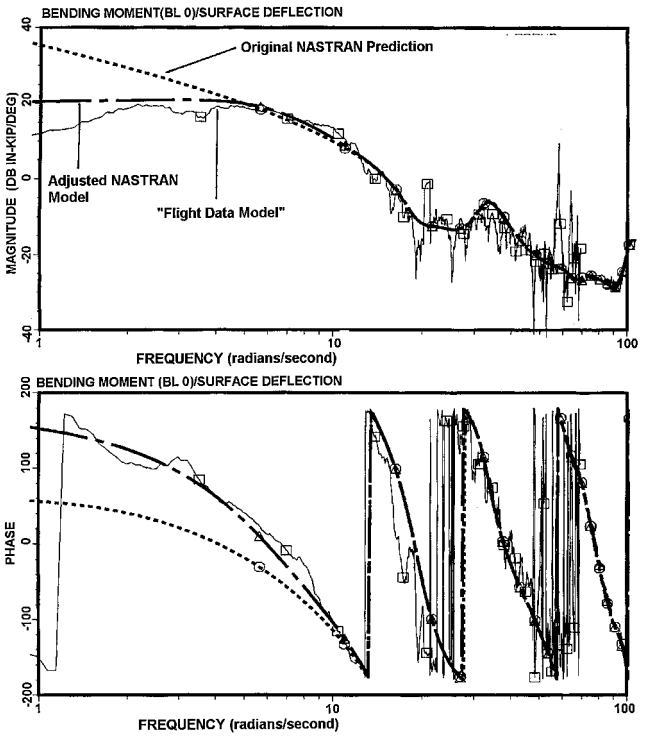

Fig. 20 Open-loop root bending to inboard elevon.

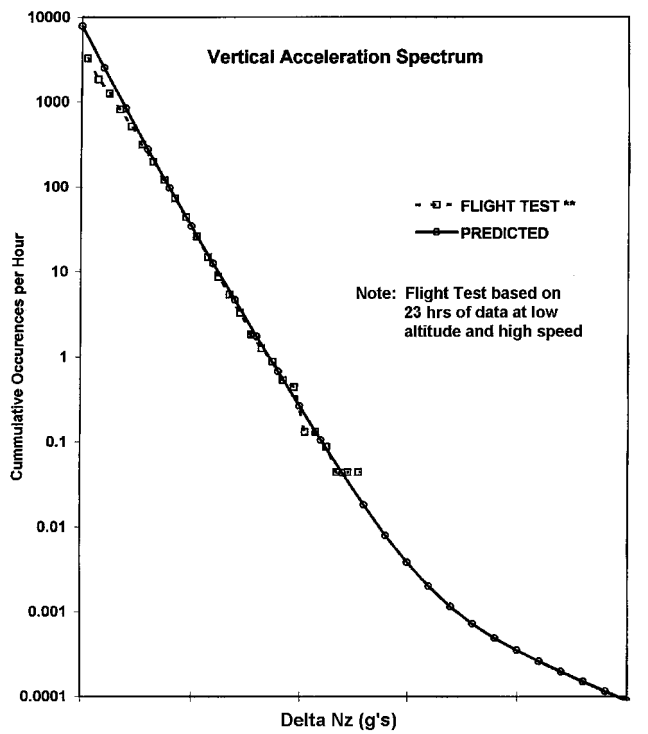

Fig. 21 *Nz* exceedance spectrum.

vehicle configurations. Figure 18 shows a relatively poor comparison due to turbulence. Degraded comparisons were also observed with large enough flight condition changes that they affected the aerodynamics or vehicle configuration.

Postflight analysis compared the FDMs with the predictions of the MSC/NASTRAN model. Flight data analysis indicated that the vehicle had more static stability than predicted. A uniform adjustment (% mean aerodynamic chord shift) in aerodynamic center was made across the span of the wing by modifying the aerodynamic weighting factors. Figures 19 and 20 show good agreement of the adjusted MSC/NASTRAN models and FDMs.

Air vehicle dynamic response characteristics were reevaluated with the revised models to verify the aircraft structure gust design loads. A formal gust loads survey was not an element of the flight-test program. The successful validation of the dynamic model provides high confidence in the final gust design loads. Flight-test experience indicates that the GLA system is performing to expectations as seen in Fig. 21, which compares Nz exceedance data to predicted results.

Conclusions

The B-2's unconventional configuration, low wing loading, broad operating envelope, and unique aeroelastic characteristics presented a number of design challenges. The design solution integrates three-axis stability augmentation and vertical GLA functions into a quad redundant digital flight control system. In addition, the graphite composite primary wing box structure is stiffness tailored to enhance dynamic response stability.

This paper outlines the multidisciplinary approach to developing the analytical models used in refining and validating the total system design. All design objectives were met and demonstrated in an extensive ground and flight test program. The aircraft exhibits outstanding handling and ride qualities throughout the flight envelope. Aeroelastic tailoring of the wing structure in combination with active load alleviation was a key factor in meeting weight goals and achieving overall performance objectives.

References

[1]Schaefer, W. S., Inderhees, L. J., and Moynes, J. F., "Flight Control Actuation System for the B-2 Advanced Technology Bomber," Society of Automotive Engineers, TP-911112, Oct. 1990.

[2]"MSC/NASTRAN Aeroelastic Supplement," MacNeal–Schwendler Corp., Pasadena, CA, June 1980.

[3]Giesing, J. P., Kalman, T. P., and Rodden, W. P., "Correction Factor Techniques for Improving Aerodynamic Prediction Methods," NASA CR-144967, May 1976.

[4]Stone, C. R., "Modelling for Control," *Proceedings for the Aeroservoelastic Specialists Meeting*, AFWAL-TR-84-3105, Vol. 2, Air Force Wright Aeronautical Lab., Dayton, OH, Oct. 1984, pp. 57–76.

[5]Roger, K. L., "Airplane Math Modeling Methods for Active Control Design," *Structural Aspects of Active Controls*, CP-228, AGARD, Aug. 1977.

[6]Thompson, P. M., "Hybrid Statistics of Sampled-Data Systems with Delays," TR 2409-9, Systems Technology, Hawthorne, CA, Oct. 1991.

[7]Jacobson, S. B., and Moynes, J. F., "Ride Qualities Criteria for the B-2 Bomber," AIAA Paper 90-3256, Sept. 1990.

[8]"Airplane Strength and Rigidity, Flight Loads," U.S. Air Force, MIL-SPEC MIL-A-008861A, March 1971.

[9]Hoblit, F. M., *Gust Loads on Aircraft: Concepts and Applications*, edited by S. Przemieniecki, AIAA Education Series, AIAA, Washington, DC, 1988, p. 166.

[10]Crimaldi, J. P., Britt, R. T., and Rodden, W. P., "Response of B-2 Aircraft to Nonuniform Spanwise Turbulence," *Journal of Aircraft*, Vol. 30, No. 5, 1993, pp. 652–659.

[11]Vanderplaats, G. N., "CONMIN—A Fortran Program for Constrained Function Minimization," NASA TM-X-62282, Aug. 1973.

[12]Britt, R. T., "Elements of the B-2 Flight Flutter Test Program," Structures and Materials Panel Specialists' Meeting on Advanced Aeroservoelastic Testing and Data Analysis, AGARD Structures and Materials Panel Specialists' Meeting, Advanced Aeroservoelastic Testing and Analysis, Rept. AGARD CP-566, Rotterdam, The Netherlands, May 1995.

[13]Sanathanan, C. K., and Koerner, J., "Transfer Function Systhesis as a Ratio of Two Complex Polynomials," *IEEE Transactions on Automatic Control*, Vol. 1, Jan. 1963, pp. 546–558.

[14]Maine, R. E., and Iliff, K. W., "User's Manual for MMLE3, a General FORTRAN Program for Maximum Likelihood Parameter Estimation," NASA TP-1563, 1980.

[15]Winther, B. A., Hagemeyer, D. A., Britt, R. T., and Rodden, W. P., "Aeroelastic Effects on the B-2 Maneuver Response," *Journal of Aircraft*, Vol. 32, No. 4, 1995, pp. 862–867.